A family of low dispersive and low dissipative explicit schemes for computing the aerodynamic noise*

Christophe Bogey† and Christophe Bailly‡

Laboratoire de Mécanique des Fluides et d'Acoustique
Ecole Centrale de Lyon & UMR CNRS 5509
BP 163, 69131 Ecully cedex, France.

Abstract

Explicit numerical methods for spatial derivation, filtering and time integration are proposed. They are developed with the aim of computing directly the aerodynamic noise, but they are not limited to this application. All the methods are constructed in the same way by minimizing the dispersion and the dissipation errors in the wave number space up to $k\Delta x=\pi/2$. They are shown to be more accurate, and also more efficient numerically, than most of the standard explicit high-order methods. Two problems involving long-range sound propagation are resolved to illustrate their respective precisions.

1. Introduction

The need of highly accurate numerical methods was recognized from the earliest stages in the development of computational aeroacoustics.[1] The propagation of sound waves in far-field requires long-time integration with minimal dissipation and dispersion. This can not be done using the low-order schemes generally used in computational fluid dynamics, and therefore new schemes were proposed. All methods for solving the compressible flow equations with accuracy and efficiency were considered. The first ones were relative to the spatial derivation with finite-difference schemes showing dispersive properties optimized in the wavenumber space: among them, the explicit Dispersion-Relation-Preserving (DRP),[2] implicit compact,[3–6] and ENO schemes.[7] The filtering which must be used to ensure numerical stability was then improved to decrease the dissipative effects on the resolved wave numbers, and both explicit[8,9] and implicit filters[3,10] were provided. Finally, time integration was also optimized for noise computation, and low-dissipation and low-dispersion Adams-Bashforth[2] and Runge-Kutta algorithms[4,11–13] were formulated. The list just drawn above is not exhaustive, and other numerical methods were improved, such as, for instance, the MacCormack schemes.[14]

The present work is in keeping up with the more general pattern of computing noise directly from the unsteady compressible Navier-Stokes equations. This approach is very attractive, since both the flow and the sound field are intended to be calculated with a high precision by the same computation. In this way, not only the sound propagation, but also the noise generation must be taken into account numerically, and the turbulent flow must especially be correctly described to provide the physical acoustic sources. This issue is of great importance using the Large Eddy Simulation (LES) approach, where the turbulent scales are calculated up to the grid cut-off wavenumber, whereas effects of the unresolved scales are modelized.[15] Application of LES for noise computation is promising,[16,17] but it is still to be investigated very carefully for high Reynolds number flows. It is actually necessary that the numerical algorithm accounts for the spectral cut-off properly,[18] by introducing negligible dissipation and dispersion on the resolved scales. This requirement is even more acute with the modellings based on dynamic procedures,[19] evaluating the subgrid terms from the smaller resolved scales. It has been demonstrated recently that numerical errors can exceed the magnitude of the subgrid terms,[20] and that a poor calculation of the smaller scales can modify significantly the contribution of these terms.[21] Thus, the use of accurate schemes is crucial as much for the flow simulation as for the sound propagation itself.

The motivation of the present work is to pro-

†Research scientist CNRS, Member AIAA, email: christophe.bogey@ec-lyon.fr

‡Assistant Professor, Member AIAA, email: christophe.bailly@ec-lyon.fr

vide the numerical methods necessary for an explicit algorithm, following the requirements listed above. Schemes are developed in the same way as those specific to computational aeroacoustics. However, instead of demanding an accuracy limit for about seven points per wavelength such as the DRP scheme,[2] the spatial-discretization methods must calculate the waves up to four points per wavelength with the aim of dynamic LES. The time-integration methods must also have better stability properties than those found in the literature.[4,11,12] Thus, central finite-difference schemes for spatial-derivation, selective filters for removing grid-to-grid oscillations, and low-storage Runge-Kutta algorithms for time advancement are optimized by minimizing their dispersion and dissipation errors for the same range of wave numbers. Test filters with characteristics improved in the wavenumber space are also proposed for LES. Great attention is drawn to develop methods with a high accuracy, but also with a high numerical efficiency to decrease their computational costs. Systematic comparisons to standard explicit methods are used, and two basic problems are proposed. The first one is a long-range propagation problem, and the second one is devoted to LES since waves with four points per wavelength are involved.

Optimized finite-difference schemes, selective filters, low-storage Runge-Kutta algorithms and test filters are presented in sections 2, 3, 4 and 5 respectively. Dispersive and dissipative properties are shown, and both numerical accuracy and efficiency are discussed. In section 6, the test problems are solved using the optimized and standard methods. Concluding remarks are given in section 7. Finally, coefficients of the optimized schemes are provided in the appendices A, B, C and D.

2. Finite-difference schemes for spatial derivation

The spatial derivative $\partial u/\partial x$ at x_0 can be approximated by a central, $2N+1$ point stencil, finite-difference scheme as

$$\frac{\partial u}{\partial x}(x_0) = \frac{1}{\Delta x}\sum_{j=-N}^{N} a_j u(x_0 + j\Delta x) \qquad (1)$$

where Δx is the spacing of a uniform mesh, and the coefficients a_j are such as $a_j = -a_{-j}$, providing a scheme with no dissipation.

For standard schemes, coefficients a_j are determined to cancel the terms of the Taylor series of (1) so that the maximum order is reached. Thus, standard schemes using 9, 11 and 13 points, hereafter referred to as FDs9p, FDs11p and FDs13p, are of order 8, 10 and 12 respectively.

In this work, following Tam & Webb,[2] schemes are constructed from their dispersion properties. By applying spatial Fourier transform to (1), the effective wave number $k^\star$ of the scheme is given by

$$k^\star \Delta x = 2\sum_{j=1}^{N} a_j \sin(jk\Delta x)$$

The dispersion error is the difference between the effective and the exact wave numbers, $k^\star$ and k.

Finite-difference schemes using 9, 11 and 13 points, referred to as FDo9p, FDo11p and FDo13p, are developed so that the dispersion error is small for a large range of wave numbers up to $k\Delta x = \pi/2$. They are fourth-order, and their coefficients a_j are defined to minimize the error defined by

$$\int_{\ln(k\Delta x)_l}^{\ln(k\Delta x)_h} |k^\star \Delta x - k\Delta x| \; d(\ln(k\Delta x))$$

where the limits are $(k\Delta x)_l = \pi/16$, and $(k\Delta x)_h = \pi/2$ for FDo9p and FDo11p, but $3\pi/5$ for FDo13p. Coefficients are provided in Appendix A.

The relation between the effective and the exact wave numbers for the three optimized schemes is shown in Figure 1, for $0 < k\Delta x < \pi$. Schemes are low dispersive as long as there is a good superposition with the line $k^\star \Delta x = k\Delta x$. Increasing the number of points, from $N=3$ to $N=6$, allows apparently to decrease the dispersion error for short waves. One must also note that grid-to-grid waves with $k\Delta x = \pi$ are not resolved by any schemes.

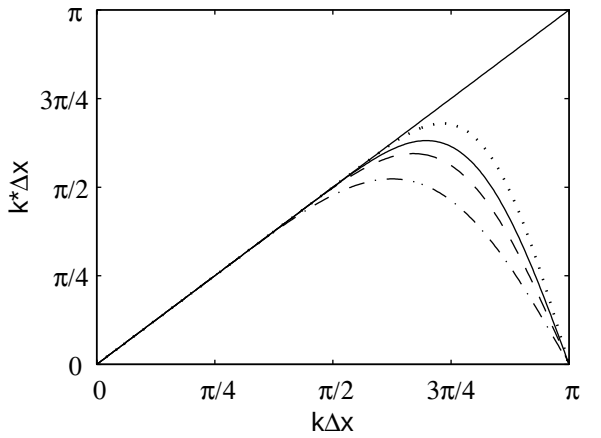

Figure 1: $k^\star \Delta x$ versus $k\Delta x$ for the optimized finite-difference schemes: – – – FDo9p (N=4), ——— FDo11p (N=5), ····· FDo13p (N=6); and – · – · for the DRP scheme of Tam & Webb[2] (N=3).

The error between the effective and the exact wave numbers, $E_k\,(k\Delta x)=|k^*\Delta x - k\Delta x|\,/\pi$, is represented in Figure 2 for $\pi/8 \leq k\Delta x \leq \pi$, in logarithmic scales. Optimized schemes are less dispersive than standard ones, for instance the FDs10p, for short waves with about $k\Delta x > \pi/4$. The reduction of the error is particularly important for wave numbers near $k\Delta x = \pi/2$, with at least one order of magnitude between optimized and standard schemes. Optimized schemes are also more dispersive for long waves but the dispersion error is then very small.

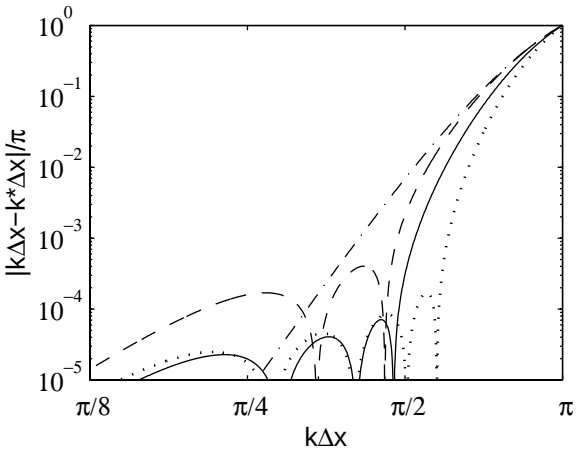

Figure 2: Dispersion error in logarithmic scales, of: – – – FDo9p, ——— FDo11p, ····· FDo13p, – · – · the standard scheme FDs11p.

To compare quantitatively the finite-difference schemes, two accuracy limits are estimated from the arbitrary criteria $E_k \leq 5\times10^{-4}$ and $E_k \leq 5\times10^{-5}$. The first limit indicates the maximum wave number properly calculated, and is expressed in term of number of points per wavelength, by $\lambda_p/\Delta x$. The second one indicates the maximum wave number accuratly calculated, and is given by $\lambda_a/\Delta x$. They are reported in Table 1 for the standard and optimized schemes. For the same $2N+1$ stencil, optimized schemes have generally better accuracy limits than standard ones. Furthermore, waves with about 4 points per wavelength are taken into account only by FDo11p and FDo13p. For these two optimized schemes, even short waves are very accuratly calculated since $\lambda_a/\Delta x \simeq 4.6$.

The numerical efficiency is now investigated through the product of the accuracy limits by the number of points $2N+1$. This quantity, corresponding to a ratio between computational cost and accuracy, must be small. Values for the standard and optimized schemes are given in Table 1. For the standard schemes, they are very similar showing that cost and accuracy vary in the same proportion. The optimized schemes, especially FDo11p and FDo13p, appear to be more efficient. For the same computational cost, they are more precise than any standard schemes.

	$\lambda_p/\Delta x$	$\lambda_a/\Delta x$	$p\lambda_p/\Delta x$	$p\lambda_a/\Delta x$
FDs9p	6.09	7.97	54.8	71.4
FDs11p	5.25	6.58	57.7	72.4
FDs13p	4.72	5.75	61.4	74.7
FDo9p	4.22	11.84	38	106.6
FDo11p	3.93	4.65	43.2	51.2
FDo13p	3.36	4.66	43.7	60.6

Table 1: Accuracy limits of the standard and optimized FD schemes for N=4, 5, 6; and product by the number of points $p=2N+1$ of the stencil. For comparison, with the DRP scheme[9]: $\lambda_p/\Delta x$=5.8 and $\lambda_a/\Delta x$=13.1.

3. Selective filters

Grid-to-grid oscillations are not solved by central finite-difference schemes, as illustrated in Figure 1, and it is necessary to remove them because they can lead to numerical instabilities. Practically, it is done by introducing artificial dissipation through additional damping terms in the equations,[22] or more efficiently, through filtering.[10,23] In the latter case, selective filters must be used to eliminate spurious short waves without affecting the physical long waves.

Applying a central, $2N+1$ point stencil filter to variable u on a uniform mesh provides

$$u^f\,(x_0) = u\,(x_0) - \sigma_d D_u\,(x_0)$$

$$\text{with} \qquad D_u\,(x_0) = \sum_{j=-N}^{N} d_j u\,(x_0 + j\Delta x) \qquad (2)$$

where coefficients d_j are such as $d_j = d_{-j}$, ensuring no dispersion, and σ_d is a constant between 0 and 1.

The standard approach[18] for determining d_j consists in cancelling the terms resulting from the Taylor series of (2) for $k\Delta x \to 0$. In this way, standard selective filters using 9, 11 and 13 points, referred to as SFs9p, SFs11p and SFs13p, are of order 8, 10 and 12 respectively.

To develop selective filters in the present work following the idea of Tam *et al.*,[8,9] the spatial Fourier transform of (2) is considered,

$$D_k\,(k\Delta x) = d_0 + \sum_{j=1}^{N} 2d_j \cos\,(jk\Delta x) \qquad (3)$$

where $D_k(k\Delta x{=}0){=}0$, and $D_k(k\Delta x{=}\pi){=}1$ for normalization. This damping function $D_k(k\Delta x)$ shows the amount of dissipation for any wave number.

Filters SFo9p, SFo11p and SFo13p, on 9, 11 and 13 points respectively, are built up by imposing small values to $D_k(k\Delta x)$ in the range $\pi/16{\leq}k\Delta x{\leq}\pi/2$. Filters SFo9p and SF13p are fourth-order and filter SFo11p second-order, and their coefficients d_j are optimized to minimize the integrated dissipation

$$\int_{\ln(\pi/16)}^{\ln(\pi/2)} D_k\,(k\Delta x)\;\; d(\ln(k\Delta x))$$

Two conditions must also be met for $0{<}k\Delta x{<}\pi$: filters must be only dissipative with $D_k{>}0$, and to limit variations of the damping function, we impose $\partial \ln(D_k)/\partial \ln(k\Delta x){\geq}$-5 for SFo9p and SFo11p, and $\partial \ln(D_k)/\partial \ln(k\Delta x){\geq}$-10 for SFo13p. Coefficients d_j are given in Appendix B.

The damping functions of the optimized filters are displayed in Figure 3. As expected, the dissipation is small for long waves and is significant for the wave numbers near $k\Delta x{=}\pi$. Increasing the number of points, from $N{=}3$ to 6, allows to construct more selective, spectral-like filters.

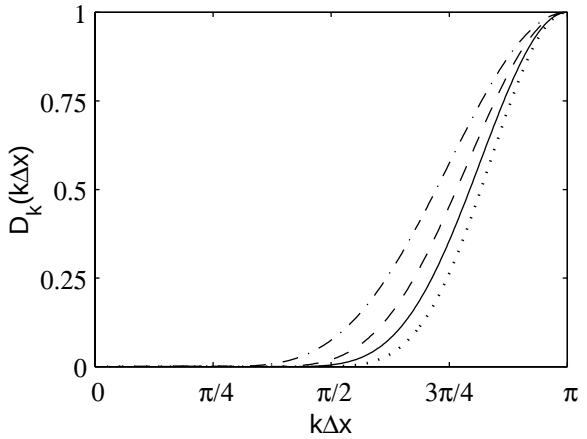

Figure 3: Damping functions of the optimized selective filters: – – – SFo9p ($N{=}4$), ——— SFo11p ($N{=}5$), ····· SFo13p ($N{=}6$); and – · – · of the optimized filter proposed by Tam *et al.*[8] ($N{=}3$).

The damping functions of the optimized filters are also represented in logarithmic scales in Figure 4, for $\pi/8{\leq}k\Delta x{\leq}\pi$, with the one of the standard filter SFs11p. Optimized filters are less dissipative for short waves with about $k\Delta x{>}\pi/4$, the difference being considerable for $k\Delta x$ close to $\pi/2$. Because of their second or fourth order, they are more dissipative for long waves but the amount of dissipation remains very small.

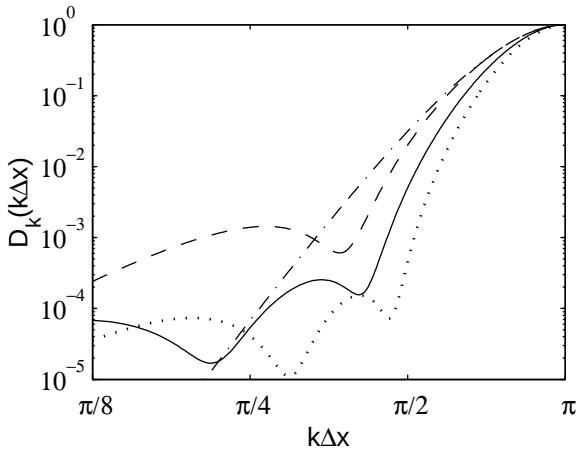

Figure 4: Damping functions in logarithmic scales, of: – – – SFo9p, ——— SFo11p, ····· SFo13p, – · – · the standard filter SFs11p.

The two criteria $\sigma_d D_k \leq 5\times10^{-4}$ and $\sigma_d D_k \leq 5\times10^{-5}$ are now used to determine the wave numbers dissipated by the selective filter in a small or in a negligible way respectively. Since filtering is applied at every iteration, it is not necessary to set $\sigma_d{=}1$, and values of σ_d between 0.1 and 0.2 are usually convenient for numerical stability. A value of $\sigma_d{=}0.2$ is chosen in the present analysis, which provides the two criteria $D_k \leq 2.5\times10^{-3}$ and $D_k \leq 2.5\times10^{-4}$. The two corresponding accuracy limits are expressed in terms of number of points per wavelength, by $\lambda_p/\Delta x$ and $\lambda_a/\Delta x$.

These limits are given in Table 2 for standard and optimized filters. Optimized filters take into account short waves in a better way than standard ones. The products of the accuracy limits by the number of points $2N{+}1$, are also provided in Table 2, and present better values for optimized filters. This demonstrates that the SFo11p and SFo13p filters are more efficient numerically.

	$\lambda_p/\Delta x$	$\lambda_a/\Delta x$	$p\lambda_p/\Delta x$	$p\lambda_a/\Delta x$
SFs9p	6.38	8.67	57.4	78
SFs11p	5.4	6.96	59.4	76.6
SFs13p	4.82	5.99	62.7	77.9
SFo9p	4.7	15.81	42.3	142.3
SFo11p	4.17	6	45.9	66
SFo13p	3.74	4.08	48.6	53

Table 2: Accuracy limits of the standard and optimized selective filters for $N{=}4,\,5,\,6$; and product by the number of points $p{=}2N{+}1$ of the stencil. For comparison, with the filter of Tam *et al.*[8]: $\lambda_p/\Delta x{=}6$ and $\lambda_a/\Delta x{=}48.6$.

4. Runge-Kutta algorithms for time integration

We now consider the time integration using Runge-Kutta algorithms of a differential equation

$$\partial u/\partial t = \mathrm{F}(u) \tag{4}$$

where the operator F is function of u. Formulations of Runge-Kutta schemes have been proposed[13,25] to improve accuracy while reducing storage requirements. It is the case for the low-storage, explicit Runge-Kutta algorithms[22,24] using only two storage locations per variable. An explicit p-stage algorithm advances the solution of equation (4) from the nth to the (n+1)th iterations as

$$\begin{array}{lcll} u^0 & = & u^n & \\ u^l & = & u^n + \alpha_l \Delta t \mathrm{F}\left(u^{l-1}\right) & \text{for } \; l = 1,..,p \\ u^{n+1} & = & u^p & \end{array}$$

where α_l are the coefficients of the algorithm, and Δt is the time step.

For F(u) linear, the algorithm is developed as

$$u^{n+1} = u^n + \sum_{j=1}^{p} \underbrace{\prod_{l=p-j+1}^{p} \alpha_l}_{\gamma_j} \Delta t^j \frac{\partial^j u^n}{\partial t^j} \tag{5}$$

A p-stage algorithm of order p can be obtained by setting γ_j=$1/j!$ for l=$1,..,p$ to match the Taylor series of $u(t_n + \Delta t)$. The standard explicit 4-stage Runge-Kutta algorithm RKs4s is defined by this way. It is fourth-order in linear, but only second order in non-linear as any scheme of this kind.

In the present work, explicit algorithms are constructed by optimizing their dispersion and dissipation properties following the idea of Hu *et al.*.[12] Assuming F(u) is linear and applying temporal Fourier transform to (5), the amplification factor of the algorithm is given by

$$G_{RK}\left(\omega\Delta t\right) = \frac{\hat{u}^{n+1}\left(\omega\right)}{\hat{u}^{n}\left(\omega\right)} = 1 + \sum_{j=1}^{p} \gamma_j \left(i\omega\Delta t\right)^j$$

For comparison with the exact amplification factor $e^{i\omega\Delta t}$, it is written as $|G_{RK}\left(\omega\Delta t\right)|\ e^{i\omega^\star\Delta t}$, where $|G_{RK}|$ is the amplification rate and $\omega^\star$ is the effective angular frequency. For the angular frequency ω, the amount of dissipation is then 1-$|G_{RK}\left(\omega\Delta t\right)|$ and the difference in phase is $\omega^\star\Delta t - \omega\Delta t$.

Two explicit 5-stage and 6-stage Runge-Kutta algorithms, respectively referred to as RKo5s and RKo6s, are built up by optimizing the dissipation and the dispersion errors up to the angular frequency $\omega\Delta t$=$\pi/2$. Both are second-order, and are defined by coefficients γ_l minimizing the following error

$$\int_{\ln(\pi/16)}^{\ln(\pi/2)} \left(1 - |G_{RK}\left(\omega\Delta t\right)|\right)\ d(\ln(\omega\Delta t)) + \int_{\ln(\pi/16)}^{\ln(\pi/2)} \left(|\omega^\star\Delta t - \omega\Delta t|/\pi\right)\ d(\ln(\omega\Delta t))$$

with these two conditions for the dissipation rate

$$\left\{ \begin{array}{l} 1 - |G_{RK}| > 0 \\ \partial[\ln(1 - |G_{RK}|)]\ /\ \partial[\ln(\omega\Delta t)] \geq -5 \end{array} \right.$$

for $0 \leq \omega\Delta t \leq \pi$, as for the selective filters. Coefficients γ_l are provided in Appendix C.

The amplification rates of the standard RKs4s and the optimized algorithms are plotted in Figure 5. Optimized algorithms are less dissipative than the standard RKs4s because their rates are close to 1 in a larger range of angular frequencies. The stability, detected for $|G_{RK}|$<1, appears also higher with the optimized algorithms.

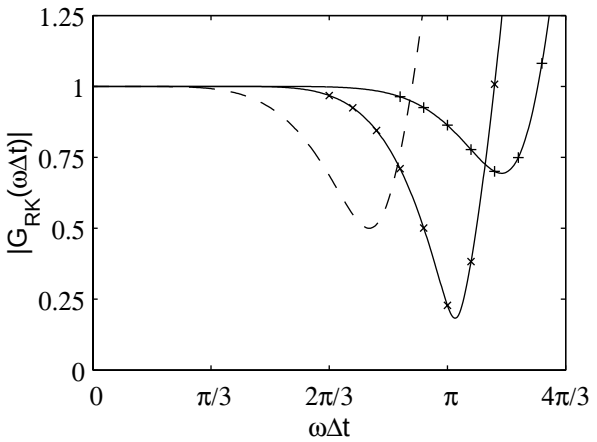

Figure 5: Amplification rates of the Runge-Kutta schemes: – – – RKs4s (p=4), ——— optimized: × RKo5s (p=5), + RKo6s (p=6).

This is demonstrated by the accuracy limits reported in Table 3, and expressed in term of number of iterations by $T_s/\Delta t$, where T_s is the period associated to the highest frequency ensuring stability for the time step Δt. The products of these limits by the number of stages are also shown in this table, and they are similar for the three algorithms. Therefore, in the case of time steps determined only from stability, the computational costs are the same. The stability of the optimized algorithms must also be compared to the poor stability of the 5-stage and

	$T_s/\Delta t$	$pT_s/\Delta t$
RKs4s	2.22	8.9
RKo5s	1.76	8.8
RKo6s	1.59	9.5

Table 3: Stability limits of the Runge-Kutta algorithms, and products by the number of stages.

6-stage algorithms proposed by Hu *et al.*[12] showing limits $T_s/\Delta t$ of 4.16 and 3.8 respectively.

The dissipation $1-|G_{RK}|$ and the phase error $E_\omega(\omega\Delta t)=|\omega^\star\Delta t-\omega\Delta t|/\pi$ of the Runge-Kutta algorithms are now represented in logarithmic scales in Figure 6. Both optimized algorithms are less dissipative and dispersive than standard RKs4s in the range $\pi/8\leq\omega\Delta t\leq\pi$, with RKo6s being also significantly more accurate than RKo5s. The improvement is spectacular for the dissipation with about one order of magnitude of difference between RKs4s and RKo5s, and between RKo5s and RKo6s.

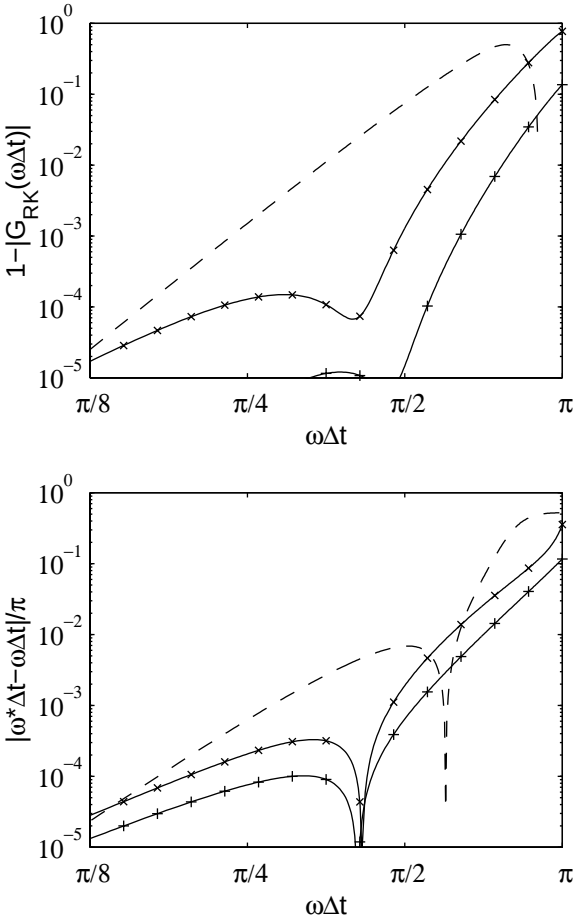

Figure 6: Dissipation and phase errors in logarithmic scales. See caption of Fig. 5 for details.

Two accuracy limits are provided in Table 4. For dissipation, the criteria $1-|G_{RK}|\leq 5\times10^{-4}$ and $1-|G_{RK}|\leq 5\times10^{-5}$ are used to determine $T_p^d/\Delta t$ and $T_a^d/\Delta t$. For phase error, the criteria $E_\omega\leq 5\times10^{-4}$ and $E_\omega\leq 5\times10^{-5}$ are applied to evaluate $T_p^\omega/\Delta t$ and $T_a^\omega/\Delta t$. The RKo5s algorithm improve the accuracy with respect to RKs4s both in dissipation and in phase, and in the same proportions. The RKo6s algorithm still decreases the phase error, but its specific feature is given by its very low dissipation compared to the other algorithms.

	$T_p^d/\Delta t$	$T_a^d/\Delta t$	$T_p^\omega/\Delta t$	$T_a^\omega/\Delta t$
RKs4s	9.65	14.24	8.41	13.69
RKo5s	4.27	11.63	4.45	13.22
RKo6s	3.29	3.76	4.11	9.69

Table 4: Accuracy limits in amplitude and phase of the Runge-Kutta algorithms.

Finally, numerical efficiencies are estimated by multiplying the accuracy limits, proportional to the number of iterations, by the number of stages, and they are displayed in Table 5. The optimized algorithms are clearly more efficient than the RKs4s. For the same computational cost, they provide more accurate results than standard RKs4s algorithm.

	$pT_p^d/\Delta t$	$pT_a^d/\Delta t$	$pT_p^\omega/\Delta t$	$pT_a^\omega/\Delta t$
RKs4s	38.6	57	33.6	54.8
RKo5s	21.4	58.2	22.2	66.1
RKo6s	19.8	22.6	24.6	58.1

Table 5: Accuracy limits multiplied by the number of stages for the Runge-Kutta algorithms.

5. Test filters

In turbulence modellings used in Large Eddy Simulation, filterings of the resolved variables are involved to determine the magnitude of the subgrid terms. Application to variable u is written, as for the grid-to-grid oscillation filters, as

$$u^f(x_0)=u(x_0)-D_u(x_0)$$

with $D_u(x_0)$ given by expression (2). Usually, the grid filter width is estimated as Δx, and test filters having an effective width of $2\Delta x$ or $3\Delta x$ are used. These filters are constrained so that their damping functions (3) are such as $D_k(k_c\Delta x)=1/2$ for $k_c\Delta x=\pi/2$ and $k_c\Delta x=\pi/3$ respectively.

To construct cut-off test filters, coefficients d_j can be evaluated by vanishing the low-order terms[18]

in the Taylor series of $D_k\,(k\Delta x)$ for $k\Delta x \to 0$, and of 1-$D_k\,(k\Delta x)$ for $k\Delta x \to \pi$. However, to obtain filters with better characteristics in the whole range of wave numbers, it is more interesting to use a minimization procedure in Fourier space. In this work, test filters with $k_c\Delta x = \pi/2$ and $k_c\Delta x = \pi/3$ are built up in this way. We impose $D_k\,(0)=0$, $D_k\,(\pi)=1$, and $D_k\,(k_c\Delta x)=1/2$. For a sharp gradient near the cut-off wave number, we also set $d_{2j}=0$ and $d_{3j}=0$ $(j\neq 0)$ respectively for the two filters. The other coefficients are optimized to minimize the error

$$\int_{\ln(\pi/16)}^{\ln(k_c\Delta x/\sqrt{2})} |D_k\,(k\Delta x)|\;\; d(\ln(k\Delta x)) + \int_{\ln(\sqrt{2}k_c\Delta x)}^{\ln(\pi)} |1 - D_k\,(k\Delta x)|\;\; d(\ln(k\Delta x))$$

The proposed test filters, TFo11p$_{\pi/2}$, TFo15p$_{\pi/2}$, TFo11p$_{\pi/3}$ and TFo15p$_{\pi/3}$, require 11 or 15 points, and their damping functions are shown in Figures 7 and 8. They appear to be selective enough to eliminate the wave numbers such as $k>k_c$ without affecting significantly the waves numbers with $k<k_c$. Coefficients d_j are provided in Appendix D.

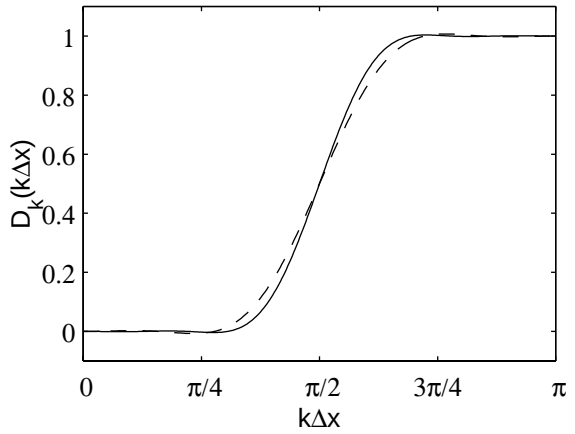

Figure 7: Damping functions of the test filters: – – – TFo11p$_{\pi/2}$ (N=5), ——— TFo15p$_{\pi/2}$ (N=7).

6. Test problems

6.1 Definition

Two basic problems are considered to illustrate the relative accuracy of the standard and the optimized schemes used for spatial derivation, grid-to-grid selective filtering and time integration. Both involve the long-range propagation of one-dimensional disturbances, allowing the observation of dispersion

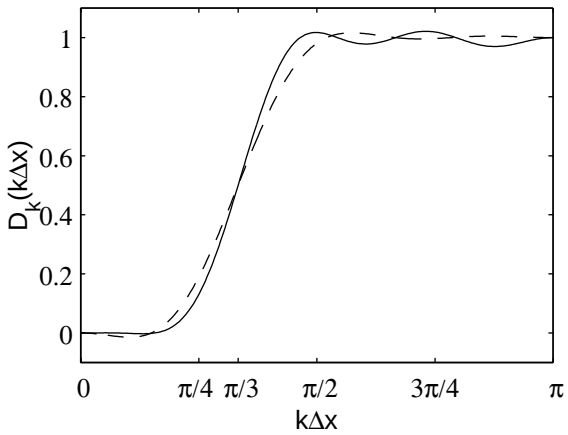

Figure 8: Damping functions of the test filters: – – – TFo11p$_{\pi/3}$ (N=5), ——— TFo15p$_{\pi/3}$ (N=7).

or dissipation errors. The convective wave equation

$$\frac{\partial u}{\partial t} + c\frac{\partial u}{\partial x} = 0 \qquad \text{with} \quad c = 1$$

is solved, with a time step derived from the mesh spacing as $\Delta t = \alpha\Delta x/c$, α being the CFL number.

Initial disturbances at $t = 0$ are defined as

$$u(x) = \sin\left(\frac{2\pi x}{a\Delta x}\right)\exp\left(-\ln(2)\left(\frac{x}{b\Delta x}\right)^2\right)$$

where $a\Delta x$ is the dominant wavelength, and $b\Delta x$ the half-width of the Gaussian function. Parameters a and b are directly connected to the spectral contents of the disturbances, and we set a=8 and b=3 for problem I, a=4 and b=9 for problem II. The normalized spatial power spectral densities of the initial disturbances are displayed in Figure 9.

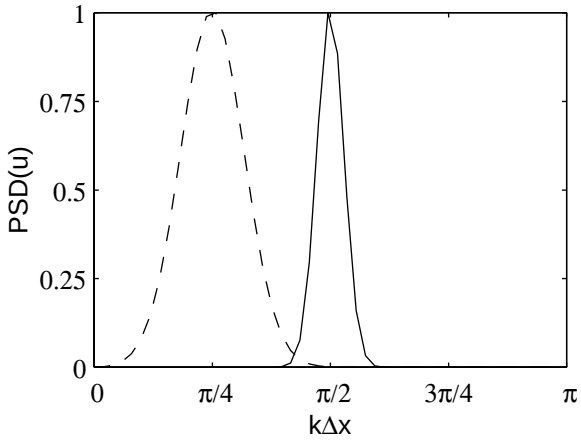

Figure 9: Spectral contents of the initial disturbances for: – – – problem I, ——— problem II.

Problem I is a typical test case to study the propagation over a large distance. The initial perturbation is characterized by wave numbers in the range $0<k\Delta x<\pi/2$ with a peak for $k\Delta x=\pi/4$, i.e. eight points per wavelength. It is propagated over $800\Delta x$ corresponding to 100 times the dominant wavelength, to emphasize possible numerical errors.

The motivation for problem II is to investigate the way the wave numbers such as $k\Delta x\simeq\pi/2$, with about four points per wavelength, are calculated. These waves are often involved in the LES dynamic procedure to evaluate the modelling constants. The initial perturbation is propagated over a distance of $200\Delta x$, corresponding to 50 times the wavelength.

For the two problems, to quantify the agreement between the exact and the calculated solutions, the error rate e_{num} is evaluated as

$$e_{num} = \left(\sum (u_{calc} - u_{exact})^2 / \sum u_{exact}^2\right)^{1/2}$$

6.2 Problem I

First, problem I is solved using the different standard and optimized finite-difference schemes, no filtering, and the RKo6s algorithm with a time step small enough to introduce negligible errors since the CFL number is α=0.2. The results obtained with the optimized schemes are shown in Figure 10. The solution using FDo9p is slightly distorted, whereas the solutions using FDo11p and FDo13p superpose fairly on the exact solution.

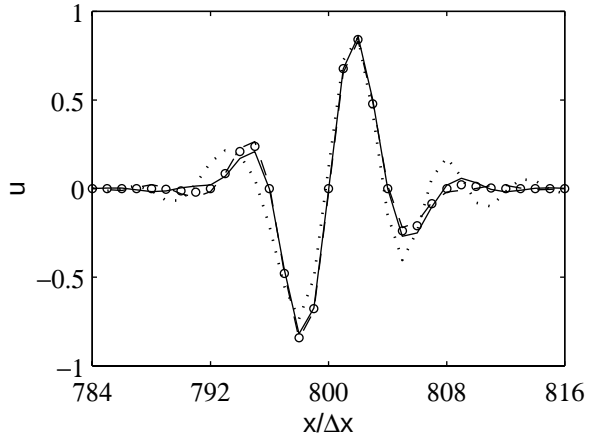

Figure 10: Problem I. ∘ exact solution; solutions using no SF, RKo6s and: ····· FDo9p, − − − FDo11p, ——— FDo13p, (α=0.2).

The agreement with the exact solution is demonstrated by the values of the numerical errors given in Table 6. Errors with the optimized schemes are at least two times lower than errors with the standard schemes using the same number of points. It should also be noted that the FDo11p scheme is very well suited to this problem.

FDs9p	0.630
FDs11p	0.307
FDs13p	0.141

FDo9p	0.329
FDo11p	0.052
FDo13p	0.065

Table 6: Problem I. Errors e_{num} using standard and optimized FD schemes, no SF and RKo6s (α=0.2).

Second, problem I is solved using the different standard and optimized selective filters, the FDo13p scheme, and the RKs6s algorithm with the same small time step as previously. Filtering is applied at every iteration with σ_d=0.2. The results calculated with the optimized filters are displayed in Figure 11 and compared to the exact solution. The solution with SFo9p is significantly dissipated, but the ones with SFo11p and SFo13p are not.

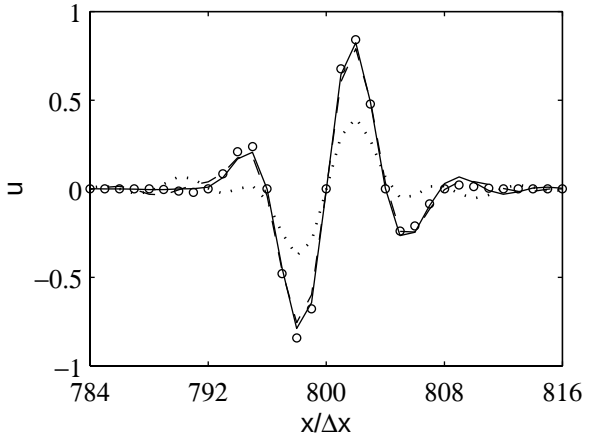

Figure 11: Problem I. ∘ exact solution; solutions using FDo13p, RKo6s and: ····· SFo9p, − − − SFo11p, ——— SFo13p, (σ_d=0.2, α=0.2).

This is supported by the values of e_{num} in Table 7. Except for SFo9p, using optimized selective filters instead of standard ones decreases remarkably the dissipation of the disturbances involved in this problem. Numerical errors with SFo13p can particularly be attributed mainly to the spatial derivation.

SFs9p	0.533
SFs11p	0.303
SFs13p	0.168

SFo9p	0.580
SFo11p	0.114
SFo13p	0.077

Table 7: Problem I. Errors e_{num} using standard and optimized SF, FDo13p and RKo6s (σ_d=0.2, α=0.2).

Third, problem I is solved using the FDo13p scheme, the SFo13p filter, and the standard or opti-

mized explicit Runge-Kutta algorithms, with CFL numbers of α=0.2, α=0.5 and α=1. Solutions for α=1 are presented in Figure 12. They are distorted and dissipated, highly with the RKs4s algorithm, but slightly with RKo5s, whereas the solution found with RKo6s is in agreement with the exact solution. The errors e_{num} are reported in Table 8. For α=0.2, the three algorithms provide very good results, but for α=0.5 and α=1, the RKo6s algorithm is quite more accurate than the two others.

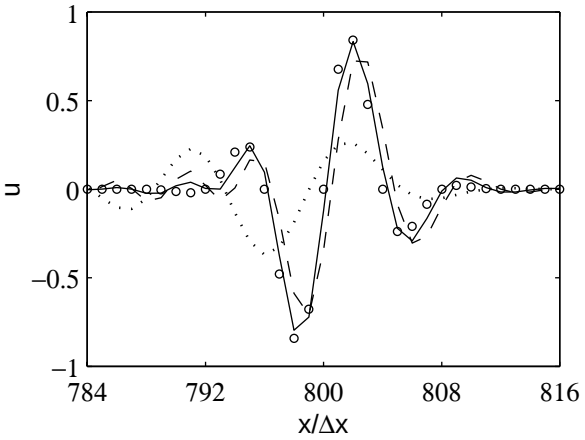

Figure 12: Problem I. ∘ exact solution; solutions using FDo13p, SFo13p and: ····· RKs4s, − − − RKo5s, ——— RKo6s, (σ_d=0.2, α=1).

	α=0.2	α=0.5	α=1
RKs4s	0.070	0.269	0.884
RKo5s	0.086	0.229	0.528
RKo6s	0.077	0.122	0.200

Table 8: Problem I. Errors e_{num} using RK schemes for different CFL numbers, FDo13p and SFo13p (σ_d=0.2).

6.3 Problem II

Problem II is solved using the RKo6s algorithm with α=0.8, and three finite-difference scheme/selective filter combinations: FDo9p and SFo9p, FDo11p and SFo11p, FDo13p and SFo13p. The solutions obtained with the two last combinations are shown in Figure 13. The wave packet is dispersed and dissipated using the 11-point methods, but it is well calculated using the 13-point methods. In the latter case, the computed solution is in phase with the exact one, and is only very slightly dissipated. The errors e_{num} given in Table 9 support these observations, and also show that the 9-point methods are not accurate enough to resolve this problem involving wave numbers with $k\Delta x \simeq \pi/2$.

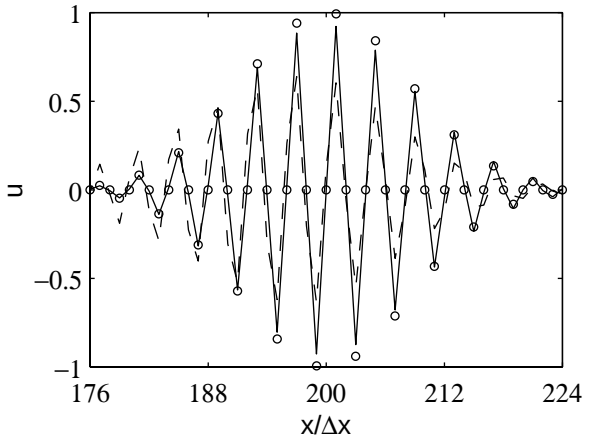

Figure 13: Problem II. ∘ exact solution; solutions using RKo6s with: − − − FDo11p and SFo11p, ——— FDo13p and SFo13p, (σ_d=0.2, α=0.8).

FDo9p + SFo9p	0.905
FDo11p + SFo11p	0.488
FDo13p + SFo13p	0.077

Table 9: Problem II. Errors e_{num} using optimized FD schemes and SF with RKo6s (σ_d=0.2, α=0.8).

7. Conclusion

A family of explicit methods including finite-difference schemes for spatial derivation, low-storage Runge-Kutta algorithms for time integration, selective filters for eliminating grid-to-grid oscillations, and test filters, is proposed. The characteristics of these methods are optimized by minimizing numerical errors for the same range of wave numbers, so that they can be associated to form algorithms with spectral-like resolution. This is of importance with the aim of performing with confidence 3-D computations, where dependence of results on numeric schemes can hardly be investigated through parametric studies. Analysis of dispersion and dissipation properties, evaluation of accuracy limits, and resolution of test problems demonstrate the higher precision of the optimized methods for short waves with respect to the standard explicit ones. Numerical efficiency is also discussed, and it is shown that for an identical computational cost, optimized methods provide higher accurate results. With this in view, the algorithm using the 11-point stencil finite-difference scheme and selective filter, and the six-stage Runge-Kutta scheme, showing stability up to a CFL number α=1.98, appears especially appropriate for computing noise.

Appendix A : Finite-difference schemes

Coefficients a_j optimized for the schemes optimized on 9, 11 and 13 points (a_0=0, a_{-j}=$-a_j$):

FDo9p	a_1	=	0.841570125482
	a_2	=	-0.244678631765
	a_3	=	0.059463584768
	a_4	=	-0.007650904064
FDo11p	a_1	=	0.872756993962
	a_2	=	-0.286511173973
	a_3	=	0.090320001280
	a_4	=	-0.020779405824
	a_5	=	0.002484594688
FDo13p	a_1	=	0.907646591371
	a_2	=	-0.337048393268
	a_3	=	0.133442885327
	a_4	=	-0.045246480208
	a_5	=	0.011169294114
	a_6	=	-0.001456501759

Appendix B : Selective filters

Coefficients d_j optimized for the filters on 9, 11 and 13 points (d_{-j}=d_j):

SFo9p	d_0	=	0.243527493120
	d_1	=	-0.204788880640
	d_2	=	0.120007591680
	d_3	=	-0.045211119360
	d_4	=	0.008228661760
SFo11p	d_0	=	0.215044884112
	d_1	=	-0.187772883589
	d_2	=	0.123755948787
	d_3	=	-0.059227575576
	d_4	=	0.018721609157
	d_5	=	-0.002999540835
SFo13p	d_0	=	0.190899511506
	d_1	=	-0.171503832236
	d_2	=	0.123632891797
	d_3	=	-0.069975429105
	d_4	=	0.029662754736
	d_5	=	-0.008520738659
	d_6	=	0.001254597714

Appendix C : Runge-Kutta algorithms

Coefficients γ_j optimized for the 5 and 6 stage algoritms:

RKo5s	γ_1	=	1
	γ_2	=	0.5
	γ_3	=	0.165250353664
	γ_4	=	0.039372585984
	γ_5	=	0.007149096448
RKo6s	γ_1	=	1
	γ_2	=	0.5
	γ_3	=	0.165919771368
	γ_4	=	0.040919732041
	γ_5	=	0.007555704391
	γ_6	=	0.000891421261

Appendix D : Test filters

Coefficients d_j optimized for the filters on 11 and 15 points with $k_c\Delta x = \pi/2$ (d_{-j}=d_j):

TFo11p$_{\pi/2}$	d_0	=	0.5
	d_1	=	-0.30399520
	d_2	=	0
	d_3	=	0.06880899
	d_4	=	0
	d_5	=	-0.01481379
TFo15p$_{\pi/2}$	d_0	=	0.5
	d_1	=	-0.30834723
	d_2	=	0
	d_3	=	0.07876835
	d_4	=	0
	d_5	=	-0.02617123
	d_6	=	0
	d_7	=	0.00575011

Coefficients d_j optimized for the filters on 11 and 15 points with $k_c\Delta x = \pi/3$ (d_{-j}=d_j):

TFo11p$_{\pi/3}$	d_0	=	2/3
	d_1	=	-0.26775782
	d_2	=	-0.12016956
	d_3	=	0
	d_4	=	0.03683622
	d_5	=	0.01775782
TFo15p$_{\pi/3}$	d_0	=	2/3
	d_1	=	-0.26598093
	d_2	=	-0.12936060
	d_3	=	0
	d_4	=	0.04602726
	d_5	=	0.03212998
	d_6	=	0
	d_7	=	-0.01614906

References

[1]Tam, C.K.W., 1995, Computational aeroacoustics: issues and methods, *AIAA Journal*, **33**(10), 1788-1796.

[2]Tam, C.K.W. and Webb, J.C., 1993, Dispersion-relation-preserving finite difference schemes for computational acoustics, *J. Comput. Phys.*, **107**, 262-281.

[3]Lele, S.K., 1992, Compact finite difference schemes with spectral-like resolution, *J. Comput. Physics*, **103**(1), 16-42.

[4]Haras, Z. and Ta'asan, S., 1994, Finite difference schemes for long-time integration, *J. Comput. Physics*, **114**, 265-279.

[5]Kim, J.W. and Lee, D.J., 1996, Optimized compact schemes with maximum resolution *AIAA Journal*, **34**(5), 887-893.

[6]Mahesh, K., 1998, A family of high order finite difference schemes with good spectral resolution, *J. Comput. Physics*, **145**, 332-358.

[7]Lockard, D.P., Brentner, K.S. and Atkins, H.L., 1995, High-accuracy algorithms for computational aeroacoustics, *AIAA Journal*, **33**(2), 246-251.

[8]Tam, C.K.W., Webb, J.C. and Dong, Z., 1993, A study of the short wave components in computational acoustics, *Journal of Comput. Acous.*, **1**(1), 1-30.

[9]Tam, C.K.W. and Shen, H., 1993, Direct computation of nonlinear acoustic pulses using high order finite difference schemes, AIAA Paper 93-4325.

[10]Visbal, M.R. and Gaitonde, D.V., 1999, High-order-accurate methods for complex unsteady subsonic flows, *AIAA J.*, **37**(10), 1231-1239.

[11]Zingg, D.W., Lomax, H. and Jurgens, H., 1996, High-accuracy finite-difference schemes for linear wave propagation, *SIAM J. on Scient. Computing*, **17**(2), 328-346.

[12]Hu, F.Q., Hussaini, M.Y. and Manthey, J.L., 1996, Low-dissipation and low-dispersion Runge-Kutta schemes for computational acoustics, *J. Comput. Phys.*, **124**, 177-191.

[13]Stanescu, D. and Habashi, W.G., 1998, $2N$-storage low dissipation and dispersion Runge-Kutta schemes for computational acoustics, *J. Comput. Physics*, **143**, 674-681.

[14]Hixon, R. and Turkel, E., 2000, Compact implicit MacCormack-type schemes with high accuracy, *J. Comput. Phys.*, **158**(1), 51-70.

[15]Lesieur, M. and Métais, O., 1996, New trends in large-eddy simulations of turbulence, *Annu. Rev. Fluid Mech.*, **28**, 45-82.

[16]Bogey, C., Bailly, C. and Juvé, D., 2000, Numerical simulation of the sound generated by vortex pairing in a mixing layer, *AIAA Journal*, **38**(12), 2210-2218.

[17]Bogey, C., Bailly, C. and Juvé, D., 2000, Computation of the sound radiated by a 3-D jet using Large Eddy Simulation, AIAA Paper 2000-2009.

[18]Vasilyev, O.V., Lund, T.S. and Moin, P., 1997, A general class of commutative filters for LES in complex geometry, *J. Comput. Physics*, **146**, 82-104.

[19]Germano, M., Piomelli, U., Moin, P. and Cabot, W.H., 1991, A dynamic subgrid-scale eddy viscosity model, *Phys, Fluids A*, **3**(7), 1760-1765.

[20]Ghosal, S., 1996, An analysis of numerical errors in Large-Eddy Simulations of turbulence, *J. Comput. Physics*, **125**, 187-206.

[21]Kravchenko, A.G. and Moin, P., 1997, On the effect of numerical errors in Large Eddy Simulations of turbulent flows, *J. Comput. Physics*, **131**, 310-322.

[22]Jameson, A., Schmidt, W. and Turkel, E., 1981, Numerical solution of the Euler equations by finite volume methods using Runge-Kutta time stepping schemes, AIAA Paper 81-1259.

[23]Kennedy, C.A. and Carpenter, M.H., 1994, Several new numerical methods for compressible shear-layer simulations, *Applied Num. Math.*, **14**(2), 397-433.

[24]Williamson, J.H., 1980, Low-storage Runge-Kutta schemes, *J. Comput. Phys.*, **35**, 48-56.

[25]Carpenter, M.H. and Kennedy, C.A., 1994, A fourth-order $2N$ storage Runge-Kutta scheme, NASA TM-109112.